Ferroelectric properties of chemically synthesized perovskite $BiFeO_3$–$PbTiO_3$ thin films

Wataru Sakamoto,[a] Asaki Iwata, and Toshinobu Yogo
Division of Nanomaterials Science, EcoTopia Science Institute, Nagoya University, Furo-cho, Chikusa-ku, Nagoya 464-8603, Japan

(Received 27 July 2008; accepted 7 October 2008; published online 19 November 2008)

Ferroelectric $BiFeO_3$–$PbTiO_3$ thin films with near morphotropic phase boundary composition were synthesized on $Pt/TiO_x/SiO_2/Si$ substrates by chemical solution deposition. Perovskite $BiFeO_3$–$PbTiO_3$ single-phase thin films were successfully fabricated at 600 °C by optimizing several processing conditions, such as the $PbTiO_3$ content. Typical ferroelectric polarization-electric field (*P-E*) hysteresis loops were observed for $(1-x)BiFeO_3$–$xPbTiO_3$ ($x=0.2$, 0.3, 0.4, 0.5) thin films, which contained some leakage current components at room temperature. In the low temperature region, the $BiFeO_3$–$PbTiO_3$ thin films demonstrated improved insulating resistance and exhibited relatively saturated *P-E* hysteresis loops. Among these films, $0.7BiFeO_3$-$0.3PbTiO_3$ thin films exhibited the largest remanent polarization, and the remanent polarization (P_r) and coercive field (E_c) at −190 °C were approximately 60 $\mu C/cm^2$ and 230 kV/cm, respectively. Furthermore, Mn doping of the $BiFeO_3$–$PbTiO_3$ thin films was effective in changing the dominant leakage current factors and improving the ferroelectric properties of the resultant thin films at room temperature. The P_r and E_c values of 5 mol % Mn-doped $0.7BiFeO_3$-$0.3PbTiO_3$ films at room temperature were approximately 40 $\mu C/cm^2$ and 100 kV/cm, respectively. Potentially large remanent polarization (~90 $\mu C/cm^2$) was also demonstrated by the BF-PT thin films. © *2008 American Institute of Physics*. [DOI: 10.1063/1.3026527]

I. INTRODUCTION

Recent research has focused on the application of ferroelectric materials with giant ferroelectric polarizations, in thin-film form, in ferroelectric random access memories, and piezoelectric and electro-optic thin-film devices. Progress in thin-film processing of several functional materials has led to the achievement of miniaturization, high integration, and high performance of electronic devices. Among the several ferroelectrics, $BiFeO_3$-based compounds have received great attention and have been extensively studied because they have both ferroelectric and ferromagnetic orderings, affording the possibility of applications in new types of devices.[1,2] $BiFeO_3$ is a well-known and representative material, with both ferroelectric ($T_C=830$ °C) and antiferromagnetic ($T_N=370$ °C) properties.[3,4] The crystallographic structure of the $BiFeO_3$ single crystal is reported to be a rhombohedrally distorted perovskite structure,[5] which provides weak ferromagnetism at room temperature because of a residual moment caused by a canted spin structure.[2,6] At −196 °C, the spontaneous polarization of $BiFeO_3$ single crystals has been reported to be 3.5 $\mu C/cm^2$ along the ⟨100⟩ direction and 6.1 $\mu C/cm^2$ along the ⟨111⟩ direction.[7] $BiFeO_3$ thin films with large remanent polarizations (>50 $\mu C/cm^2$) were fabricated by pulsed laser deposition with precise oxygen-partial-pressure control.[1,8,9] $BiFeO_3$ thin films, chemically deposited using an alcohol solution, were also shown to possess improved saturation properties of P_r and E_c, which were modified by the doping of rare earth ions.[10–12] However, in general, the preparation of pure $BiFeO_3$ compounds without impurity phases is difficult due to the low stability of Bi in perovskite $BiFeO_3$. For thin-film fabrication, the $BiFeO_3$ phase is often crystallized on substrates, along with the formation of a Bi-deficient second phase, such as $Bi_2Fe_4O_9$. The formation of $Bi_2Fe_4O_9$ tends to degrade the surface morphology owing to an exaggerated grain growth, leading to poor electrical properties.[13] Therefore, the crystallization of perovskite $BiFeO_3$ single phase is indispensable for fabricating thin films with desired performance. Moreover, $BiFeO_3$ films usually exhibit a relatively large leakage current density, which might be attributed to the oxygen vacancies induced by the volatilization of Bi, as reported in case of the $Bi_4Ti_3O_{12}$ system.[14,15] The involved reduction in Fe^{3+} to Fe^{2+} might affect the low electrical resistivity of $BiFeO_3$ thin films.[1,16–18] Thus, the observation of well-saturated ferroelectric polarization-electric field (*P-E*) hysteresis loops is quite difficult, and improvements in the structural stability and insulating resistance of $BiFeO_3$ are absolutely necessary for practical applications of $BiFeO_3$.

The $BiFeO_3$–ABO_3 solid solution systems have attracted great attention as a solution for improved structural stability. Among perovskite ABO_3 compounds, $PbTiO_3$ is a stable ferroelectric perovskite oxide with a Curie temperature of 490 °C. A solid solution of $BiFeO_3$ and $PbTiO_3$ was reported to exhibit high Curie temperatures from the ferroelectric to paraelectric phases.[19] A $(1-x)BiFeO_3$–$xPbTiO_3$ system is expected to provide the desired structural stabilization, and its electrical properties can be enhanced using the morphotropic phase boundary (MPB). According to the previous studies, the MPB of the $(1-x)BiFeO_3$–$xPbTiO_3$ system is

[a]Electronic mail: sakamoto@esi.nagoya-u.ac.jp.

located around the $x=0.3$ composition.[19–21] Furthermore, the La- and Ga-modified $BiFeO_3-PbTiO_3$ ceramics have excellent ferroelectric and piezoelectric properties near the MPB composition, separating the rhombohedral and tetragonal phases.[22]

On the other hand, the substitution of various ions in the Fe-site of $BiFeO_3$ thin films has been examined for improving the insulating resistance. Mn- and Cr-doped $BiFeO_3$ thin films demonstrated improved ferroelectric properties, probably resulting from the reduced leakage current.[23,24] These results indicate that Fe-site substitution can be a good solution for fabricating $BiFeO_3-PbTiO_3$ thin films with good electrical properties.

These facts make a modified $BiFeO_3-PbTiO_3$ solid solution with near MPB composition attractive for applications requiring excellent temperature stability properties, such as in ferroelectric, piezoelectric, and novel thin-film devices. Therefore, in this work, the fabrication and characterization of perovskite $(1-x)BiFeO_3-xPbTiO_3$ ($x=0.2$, 0.3, 0.4, 0.5) thin films with near MPB composition, on Si-based substrates, have been performed by chemical solution deposition (CSD). A CSD process using metal-organic compounds is expected to provide high homogeneity, fabrication at low temperatures, and precise control of the chemical composition. The crystallization, surface morphology, and ferroelectric properties of the chemically derived perovskite $BiFeO_3-PbTiO_3$ thin films on $Pt/TiO_x/SiO_2/Si$ substrates were examined. Furthermore, Mn doping of the $BiFeO_3-PbTiO_3$ thin films was investigated as a method for improving the ferroelectric properties of the resultant thin films at near room temperature.

II. EXPERIMENTAL DETAILS

$Bi(O^tC_5H_{11})_3$, $Fe(OC_2H_5)_3$, $Pb(CH_3COO)_2$, $Ti(O^iC_3H_7)_4$, and $Mn(O^iC_3H_7)_2$ (Kojundo Chemical, Japan) were selected as starting materials for the preparation of $(1-x)BiFeO_3-xPbTiO_3$ ($x=0.2$, 0.3, 0.4, 0.5) (BF-100xPT) precursor solutions. When Mn-doped BF-PT thin films were fabricated, the chemical compositions of the precursor solutions were set at $(1-x)Bi(Fe_{1-y}Mn_y)O_3-xPbTiO_3$ ($x=0.2$, 0.3, 0.4, 0.5, $y=0$, 0.01, 0.03, 0.05) ($BF_{1-y}M_y-100x$PT). 2-methoxyethanol, as a solvent, was dried over with molecular sieves and distilled before use. Amounts of $Bi(O^tC_5H_{11})_3$, $Fe(OC_2H_5)_3$, $Pb(CH_3COO)_2$, $Ti(O^iC_3H_7)_4$, and $Mn(O^iC_3H_7)_2$, corresponding to the desired compositions, with 3 mol % of excess Bi and 5 mol % of excess Pb, were dissolved in absolute 2-methoxyethanol. Then, the mixed solution was refluxed for 20 h, yielding a 0.2M homogeneous brown-colored precursor solution. Since the starting metal-organic compounds are extremely sensitive to moisture, the entire procedure was conducted in a dry nitrogen atmosphere.

The $BiFeO_3-PbTiO_3$ (BF-PT) thin films were fabricated using the precursor solution by spin coating at 2500 rpm for 30 s on $Pt/TiO_x/SiO_2/Si$ substrates. As-deposited BF-PT precursor films were dried at 150 °C for 5 min and calcined at 400 °C at a rate of 10 °C/min for 1 h in an oxygen flow. After five drying and calcining cycles, the calcined layers were crystallized at various temperatures by rapid thermal annealing for 1 h in an oxygen flow. The coating and calcining cycles were repeated ten times (including two heat treatments for crystallization) until the film thickness reached approximately 500 nm. The processing conditions for the thin-film fabrication were optimized compare to a former report by the authors.[21]

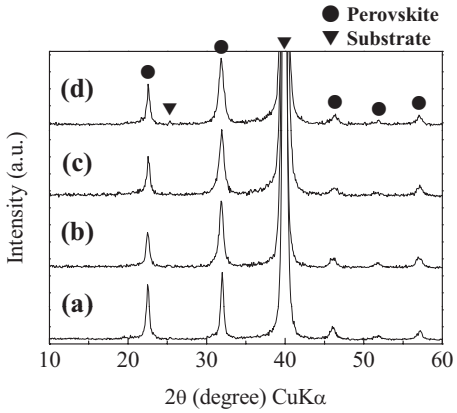

FIG. 1. XRD patterns of the $(1-x)BiFeO_3-xPbTiO_3$ (BF-100xPT) thin films on $Pt/TiO_x/SiO_2/Si$ substrates after heat treatment at 600 °C. (a) BF-20PT, (b) BF-30PT, (c) BF-40PT, and (d) BF-50PT.

The crystallographic phases of prepared BF-PT thin films were characterized by x-ray diffraction (XRD) (Rigaku, RAD RC) analysis using Cu $K\alpha$ radiation with a monochromator. The surface morphology and thickness of the crystallized thin films were observed by atomic force microscopy (AFM) (SII NanoTechnology, SPI3800N) and scanning electron microscopy (JOEL, JSM-5600), respectively. The electrical properties of the film were measured using Pt top electrodes of 3.14×10^{-4} cm^2, deposited by dc sputtering onto the surface of BF-PT films, followed by annealing at 400 °C for 1 h. The Pt layer of the $Pt/TiO_x/SiO_2/Si$ substrates was used as a bottom electrode. The electrical properties of BF-PT thin-film capacitors were evaluated with an impedance/gain phase analyzer (SI-1260, Toyo Corp.) and a ferroelectric test system (FCE-1, Toyo Corp.) at room temperature. The leakage current density-electric field (J-E) characteristics of the BF-PT thin films were characterized with an electrometer/high resistance meter (Keithley Instruments, Model 6517A). Measurement of the ferroelectric properties of the thin films at low temperature was conducted in a wafer cryostat (Sanwa, WM-363–1) under vacuum (1.0 Pa).

III. RESULTS AND DISCUSSION

A. Crystallization of BF-PT thin films on substrates

Figure 1 shows XRD patterns of the $(1-x)BiFeO_3-xPbTiO_3$ (BF-100xPT, $x=0.2$, 0.3, 0.4, 0.5) thin films, fabricated on $Pt/TiO_x/SiO_2/Si$ substrates after heat treatment at 600 °C. Although the crystallographic phase was similar to cubic (pseudocubic), BF-20PT, BF-30PT, BF-40PT, and BF-50PT thin films crystallized in perovskite BF-PT single phase with random orientation. When the BF-PT thin films with a $PbTiO_3$ content less than 20 mol % were fabricated under similar conditions, diffrac-

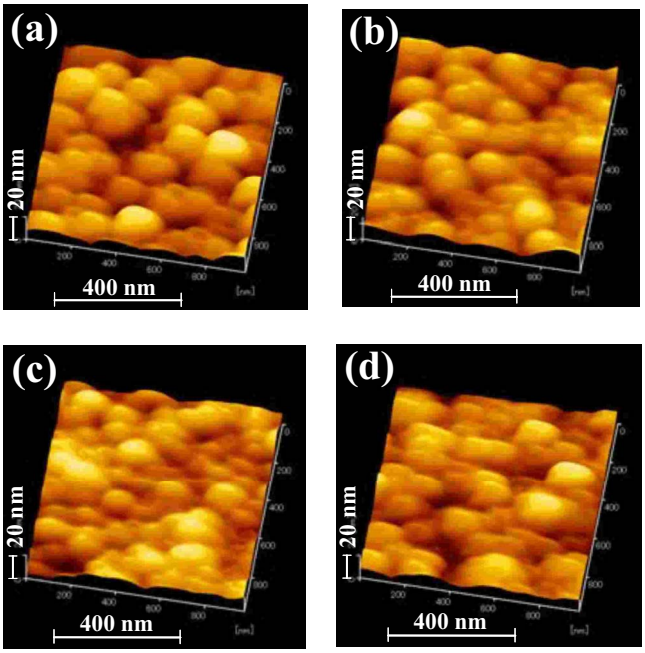

FIG. 2. (Color online) AFM images of the $(1-x)BiFeO_3-xPbTiO_3$ (BF-100xPT) thin films on $Pt/TiO_x/SiO_2/Si$ substrates after heat treatment at 600 °C. (a) BF-20PT, (b) BF-30PT, (c) BF-40PT, and (d) BF-50PT.

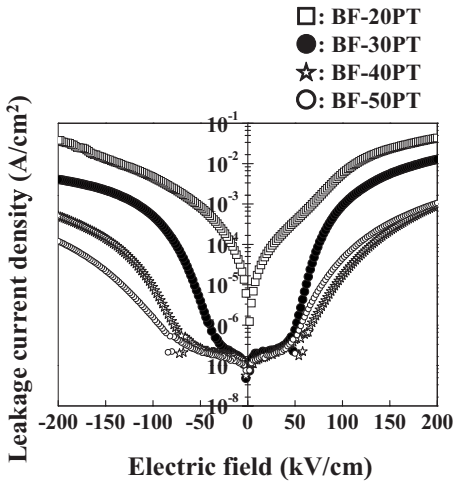

FIG. 3. The leakage current density of the $(1-x)BiFeO_3-xPbTiO_3$ (BF-100xPT) thin films on $Pt/TiO_x/SiO_2/Si$ substrates after heat treatment at 600 °C (measured at room temperature). (a) BF-20PT, (b) BF-30PT, (c) BF-40PT, and (d) BF-50PT.

tions corresponding to the second phases, such as $Bi_2Fe_4O_9$, were observed with those of perovskite BF-PT in their XRD profiles. Crystallization in perovskite BF-PT is seems to be due to the stabilization of the perovskite phase by the formation of a solid solution with $PbTiO_3$. Moreover, at a crystallization temperature of 700 °C, the BF-20PT thin films with a relatively low $PbTiO_3$ content crystallized in a mixture of perovskite BF-PT and $Bi_2Fe_4O_9$. The formation of second phases, such as the $Bi_2Fe_4O_9$ phase, is attributed to the low structural stability of perovskite BF-PT and the volatility of Bi and Pb ions at high temperature. In BF-PT systems, the stability of the perovskite phase is believed to decrease with an increase in $BiFeO_3$ concentration. On the other hand, BF-30PT, BF-40PT, and BF-50PT thin films crystallized in single-phase BF-PT at 600–700 °C, which was supported by an absence of diffraction of the second phase in this composition range. This is because an increase in $PbTiO_3$ concentration in BF-PT enlarged the process window for the synthesis of perovskite single-phase BF-PT thin films.

B. Surface morphology of BF-PT thin films

Figure 2 shows AFM images of the $(1-x)BiFeO_3-xPbTiO_3$ (BF-100xPT, $x=0.2$, 0.3, 0.4, 0.5) thin films prepared at 600 °C on $Pt/TiO_x/SiO_2/Si$ substrates. These images show that the surface morphology of the BF-PT thin films did not depend greatly on the PT content within this composition range. A tendency toward larger grain size distribution was observed in the films with increasing $PbTiO_3$ ratio. The root-mean-square (rms) roughness values of the BF-20PT, BF-30PT, BF-40PT, and BF-50PT thin films, as demonstrated in Fig. 2, were 2.8, 3.5, 2.5, and 2.6 nm, respectively. As the crystallization temperature increased, the surface morphology of the BF-20PT thin films degraded. The BF-20PT thin films, in particular, crystallized at higher temperatures, exhibiting a larger rms roughness (>10 nm). This might be due to the exaggerated grain growth through the formation of the second phase (e.g., $Bi_2Fe_4O_9$) accompanied by the volatilization of Bi and Pb ions. Tyholdt *et al.* reported exaggerated grain growth of chemically derived BF thin films, accompanied by the formation of a second ($Bi_2Fe_4O_9$) phase.[13] Although the grain growth proceeded with increasing heat treatment temperature, the rms roughness of the perovskite BF-30PT, BF-40PT, and BF-50PT thin films was smaller than 10 nm, and the surface morphology did not change much over the crystallization temperatures. Therefore, the stabilization of perovskite phase is important for the fabrication of BF-PT thin films with good surface morphology, without exaggerated grain growth, over a wide temperature range. Based upon the XRD and AFM data, the BF-PT thin films prepared at 600 °C were selected for comparison of their electrical properties, especially the ferroelectric properties of the BF-PT thin films with various $PbTiO_3$ content.

C. Leakage current and ferroelectric properties of the BF-PT thin films

The BF-based thin films tend to exhibit low insulating resistance, therefore, analysis of their leakage current behavior is very important. The composition dependence of leakage current properties at room temperature was investigated. Figure 3 shows the leakage current density of the BF-PT thin films as a function of the electric field. Although all the films exhibited low insulating resistance, their leakage current density was decreased with increasing PT content. The formation of a solid solution with PT leads to the stabilization of the perovskite structure and a reduction in the effects of the oxygen vacancy, accompanied by volatilization of Bi or Pb. Leakage current behavior of typical ferroelectric thin films was observed in case of the BF-PT thin films with a $PbTiO_3$ above 30 mol %. However, the leakage current densities of the films showed an abrupt increase with the applied field at 50–60 kV/cm. Moreover, all the samples exhibited

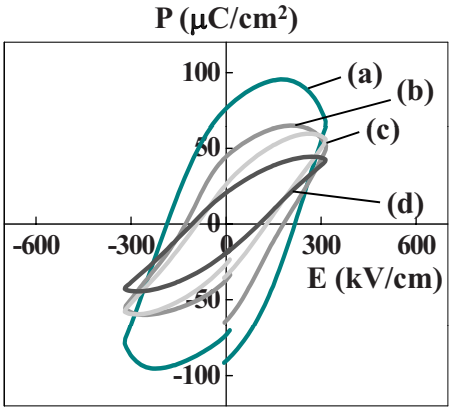

FIG. 4. (Color online) *P-E* hysteresis loops of the $(1-x)BiFeO_3-xPbTiO_3$ (BF-100*x*PT) thin films on $Pt/TiO_x/SiO_2/Si$ substrates after heat treatment at 600 °C (measured at room temperature). (a) BF-20PT, (b) BF-30PT, (c) BF-40PT, and (d) BF-50PT.

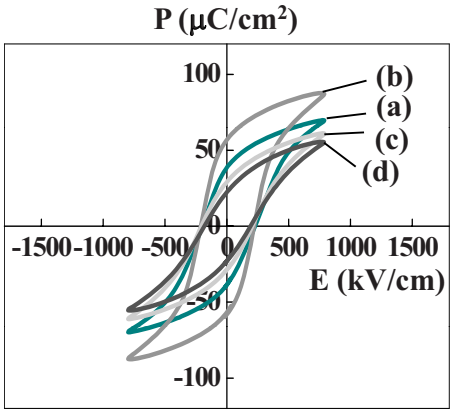

FIG. 5. (Color online) *P-E* hysteresis loops of the $(1-x)BiFeO_3-xPbTiO_3$ (BF-100*x*PT) thin films on $Pt/TiO_x/SiO_2/Si$ substrates after heat treatment at 600 °C (measured at −190 °C). (a) BF-20PT, (b) BF-30PT, (c) BF-40PT, and (d) BF-50PT.

asymmetric behavior in the direction of the applied electric field. This might be due to the complicated defect structure of the films, the Pb, Bi, and oxygen vacancies seem to be distributed nonuniformly in the thickness direction. Detailed leakage current mechanisms are discussed in Sec. III D.

P-E hysteresis measurements were also performed to characterize the ferroelectric property of the $(1-x)BiFeO_3-xPbTiO_3$ (BF-100*x*PT, $x=0.2$, 0.3, 0.4, 0.5) thin films crystallized at 600 °C. Figure 4 shows the *P-E* hysteresis loops of the $(1-x)BiFeO_3-xPbTiO_3$ (BF-100*x*PT, $x=0.2$, 0.3, 0.4, 0.5) thin films measured at room temperature. Although all the films showed ferroelectric hysteresis loops, saturated *P-E* loops were not observed in any film because of the large leakage current in the high electric field region. The leakage current components of the *P-E* loops depended on the PT content, which is reflected in the leakage current density curves of the films, as demonstrated in Fig. 3. One of the major problems of $BiFeO_3$-based thin films is their low electrical resistivity, which makes the measurement of their ferroelectric properties at room temperature difficult. This is mainly due to the oxygen vacancies, accompanied by the volatilization of Bi and Pb. In addition, the reduction in Fe^{3+} to Fe^{2+} might degrade the insulation resistance in the films. To suppress the conductivity and reveal the potential polarization in the BF-PT thin films, measurement was performed at low temperature. Figure 5 shows the *P-E* hysteresis loops of the $(1-x)BiFeO_3-xPbTiO_3$ (BF-100*x*PT, $x=0.2$, 0.3, 0.4, 0.5) thin films measured at −190 °C. These thin films showed well-shaped ferroelectric hysteresis loops with no leakage current component, compared to those at room temperature (Fig. 4). Among these films, the BF-30PT thin films showed the largest polarization. The remnant polarization (P_r) and coercive field (E_c) of the 600 °C-prepared BF-30PT thin films were approximately 60 $\mu C/cm^2$ and 230 kV/cm^2, respectively. The 600 °C-prepared BF-20PT, BF-40PT, and BF-50PT thin films exhibited P_r values smaller than 40 $\mu C/cm^2$. These P_r values were higher than those reported for the La- and Ga-modified BF-PT bulk ceramics, and were as good or better than those of the BF-PT thin films fabricated by pulsed laser deposition with near MPB compositions.[19,25] However, the E_c values of the BF-PT films were inferior to those of the BF-PT-based ceramics. Improvements in the insulating resistance and ferroelectric properties at ambient temperature are necessary for practical application of the BF-PT thin films.

D. Change in the leakage current properties of the BF-PT thin films by Mn doping

Mn-doped BF-PT thin films were fabricated in the same manner as the BF-PT films, and the effects of Mn doping on the leakage current properties and ferroelectric properties at room temperature were investigated, as well as for the reported Mn-doped BF thin films.[24] The Mn ion has an ionic radius similar to that of the Fe ion, and therefore, is easily introduced into the perovskite lattice. All the Mn-doped BF-PT thin films were crystallized in the single phase of perovskite BF-PT, similar to the nondoped BF-PT thin films, as shown in Fig. 1. Figure 6 shows the leakage current density of the Mn-doped BF-30PT thin films crystallized at 600 °C with various amounts of Mn as a function of the electric field. In this case, the Mn content doped for the Fe-

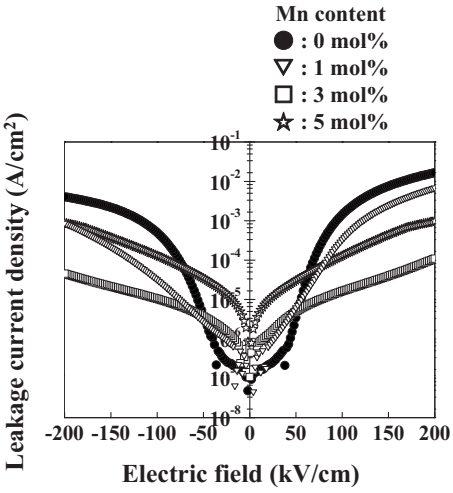

FIG. 6. The leakage current density of the Mn-doped $0.7BiFeO_3$-$0.3PbTiO_3$ thin films on $Pt/TiO_x/SiO_2/Si$ substrates after heat treatment at 600 °C (measured at room temperature). Mn content: (a) 0 mol %, (b) 1 mol %, (c) 3 mol %, and (d) 5 mol %.

site was 1, 3, and 5 mol %, and these Mn-doped BF-30PT thin films are described as $BF_{0.99}M_{0.01}$-30PT, $BF_{0.97}M_{0.03}$-30PT, and $BF_{0.95}M_{0.05}$-30PT, respectively. As shown in Fig. 6, above 3 mol % Mn doping of the BF-30PT films produced a definite change in the leakage current behavior, while a Mn content of 1 mol % was less effective. Increasing the amount of Mn doping produced lower leakage current density in the higher electric field region (>50 kV/cm), and higher leakage current density in the lower electric field region (<60 kV/cm), as demonstrated in Fig. 6. This tendency is consistent with that of the Mn-doped $BiFeO_3$ (Ref. 24) and $SrTiO_3$ (Ref. 26) thin films reported by Singh *et al.* and Morito *et al.* The electrical conductivity of Mn-doped BF-PT thin films (more than 3 mol %) increased as the amount of Mn dopant increased, as reported by several researchers.[24,27] Moreover, improvement of the symmetric properties of the *J-E* curves in positive (from bottom to upper electrode) and negative (from upper to bottom electrode) applied field directions was also observed with Mn doping. This is due to the change in the dominant factor, which determines the leakage current from the interface-limited (between the film and electrode) to bulk-limited (BF-PT film) conduction.

Possible leakage current mechanisms for the ferroelectric perovskite oxide thin films are two categorized as interface-limited and bulk-limited conductions. Of all the possible mechanisms typically observed in the ferroelectric perovskite oxide thin films, based upon the data shown in Fig. 6, interface-limited Schottky emission[26,28–30] is considered to be the first mechanism. The plots for $E^{1/2}$ in ln J for 0 and 1 mol % Mn-doped BF-30PT thin films in the applied field area of Fig. 6 are shown in Fig. 7(a). Since a straight fit to the data in Fig. 7(a) can be possible in relatively low applied field area, Schottky emission is the dominant leakage mechanism for these thin films within this electric field region. The plots for $E^{1/2}$ in ln J/E of the films with 0, 1, 3, and 5 mol % Mn doping are also shown in Fig. 7(b). When the amounts of Mn doping are 1, 3, and 5 mol %, the straight lines following the Poole–Frenkel trap-limited conduction[28–30] appear similar to that of the nondoped BF-PT film (0 mol %) over 100 kV/cm. This conduction mechanism involves consecutive hopping of charges between defect trap centers. The ionization of the trap charges can be both thermal and field activated.[30] To identify the mechanism that dominates the leakage current, it is necessary to calculate the dielectric constant from the slopes of these plots.[28–30] The dielectric constants of the BF-30PT films with and without Mn doping, obtained from the Poole–Frenkel plot [Fig. 7(b)], are found to be approximately 6.25 which is close to the expected value of the reported dielectric constant.[28–30] This indicates that the leakage mechanism in these BF-PT films is dominated by the Poole–Frenkel emissions. Similar behavior of the Poole–Frenkel emission has been recognized as the dominant leakage mechanism in lead-based thin-film ferroelectric capacitors.[29,31] In case of BF-PT, the likely trap center is considered to be the Fe ions. It is widely accepted that oxygen vacancies were formed during heating cause a portion of the Fe^{3+} ions to transform into

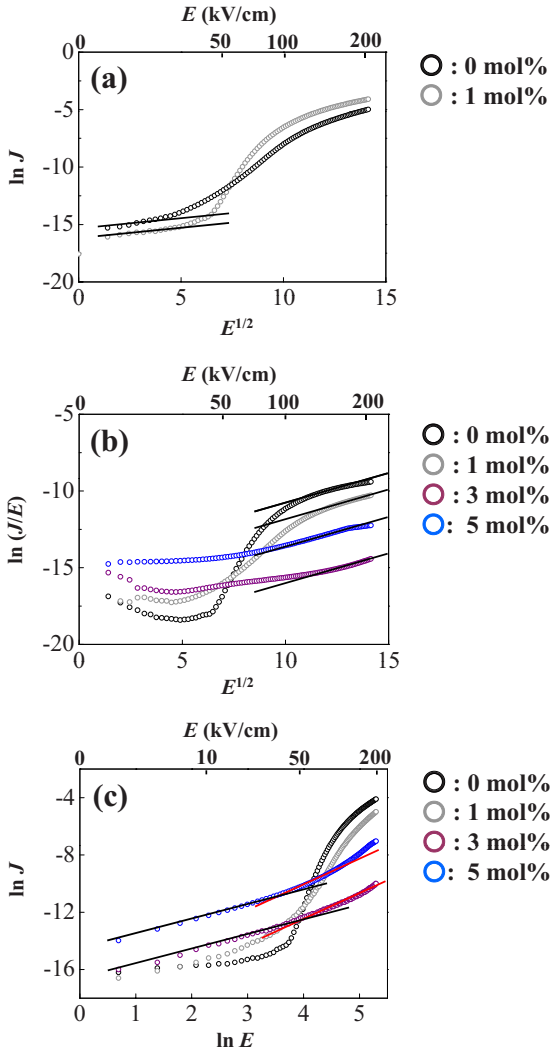

FIG. 7. (Color online) (a) ln J vs $E^{1/2}$, (b) ln(J/E) vs $E^{1/2}$, and (c) double logarithm plots for the Mn-doped $0.7BiFeO_3$-$0.3PbTiO_3$ thin films on $Pt/TiO_x/SiO_2/Si$ substrates after heat treatment at 600 °C (measured at room temperature).

Fe^{2+}. These Fe ions are often thought to be responsible for the high leakage current of the BF-based compounds.

On the other hand, at an applied field less than around 100 kV/cm, the leakage current properties of the $BF_{0.97}M_{0.03}$-30PT, and $BF_{0.95}M_{0.05}$-30PT films did not match either of these two mechanisms. The leakage current behavior in the BF-30PT exhibited remarkable changes with a Mn concentration above 3 mol % in this study. Therefore, the ln J-ln E plot of the Mn-doped BF-30PT thin films in the applied field area of Fig. 6 is characterized to examine the difference in the leakage current mechanism from Mn doping above 3 mol %, as demonstrated in Fig. 7(c). When the amount of Mn doping exceeded 3 mol %, Ohmic conduction[26,28] was observed in a low applied field range (<50 kV/cm), and the conduction mechanism changed slightly for more than 50 kV/cm. This indicates that the influence of Schottoky-thermionic emission at the interface area on the leakage current properties is reduced by Mn doping to BF-PT thin films even with a high work function Pt electrode. The results showed that, in an electric field below 50 kV/cm, the leakage current density of the

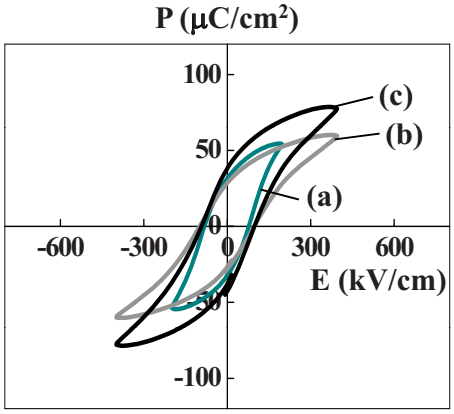

FIG. 8. (Color online) *P-E* hysteresis loops of the Mn-doped $0.7BiFeO_3$-$0.3PbTiO_3$ thin films on $Pt/TiO_x/SiO_2/Si$ substrates after heat treatment at 600 °C (measured at room temperature). Mn content: (a) 1 mol %, (c) 3 mol %, and (d) 5 mol %.

$BF_{0.97}M_{0.03}$-30PT and $BF_{0.95}M_{0.05}$-30PT thin films followed typical Ohmic conduction behavior, rather than the Schottky emission as observed in the case of BF-30PT and $BF_{0.99}M_{0.01}$-30PT thin films, which is confirmed by the slope of ln *J*-ln *E* ($n \approx 1$).[24,27,32] However, Ohmic conduction was not dominant in a high electric field region when the Mn doping increased to 5 mol %. It was found that conduction from another mechanism, such as space-charge-limited current conduction,[26,28–30] became dominant from 50 to 100 kV/cm. The gradients of the fitting line [in Fig. 7(c)] were nearly 2.0 at an applied field of over 50 kV/cm. As previously mentioned, at a higher applied field over 100 kV/cm, the Poole–Frenkel conduction was observed as the dominant leakage mechanism similar to the BF-30PT and $BF_{0.99}M_{0.01}$-30PT thin films [Fig. 7(b)].

As can be seen from Fig. 6, in the BF-30PT and $BF_{0.99}M_{0.01}$-30PT thin films, the leakage current density increased steeply with an applied field of over 50 kV/cm, whereas the $BF_{0.97}M_{0.03}$-30PT and $BF_{0.95}M_{0.05}$-30PT thin films maintained a lower leakage current in higher applied field regions. In this case, doped Mn might play an important role as an acceptor of the hopping electrons between Fe^{3+} and Fe^{2+} in the BF-PT film. These facts affect the ferroelectric properties of the synthesized BF-PT thin films. The temperature dependence of the leakage current behavior must be evaluated to determine the optimum amount of Mn and to clarify the mechanisms. This will be carried out in near future.

E. Improved ferroelectric properties of the BF-PT thin films due to Mn doping

Figure 8 demonstrates *P-E* hysteresis loops of the $BF_{0.99}M_{0.01}$-30PT, $BF_{0.97}M_{0.03}$-30PT, and $BF_{0.95}M_{0.05}$-30PT thin films measured at room temperature. The Mn-doped BF-30PT thin films exhibited hysteresis loops with little leakage component, compared to those of the BF-30PT thin film, as shown in Fig. 4. This suggests that Mn doping of the BF-30PT thin films is very effective in improving the electrical resistivity for evaluating intrinsic polarization property. In the $BF_{0.99}M_{0.01}$-30PT thin films, only an electric field smaller

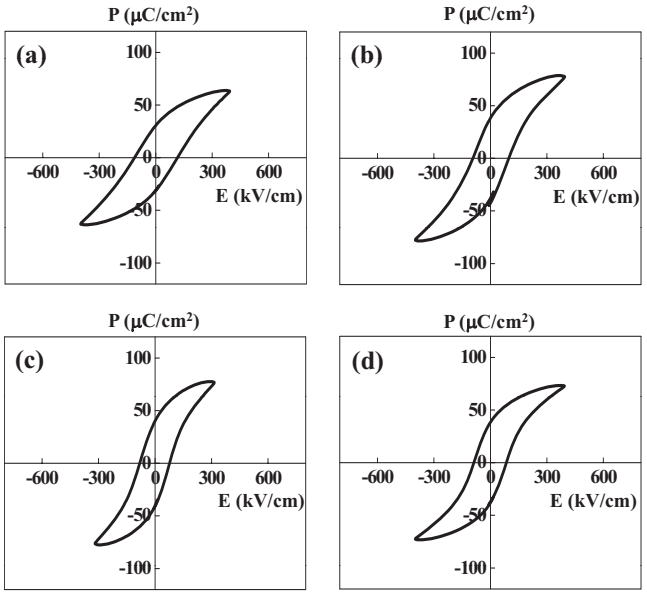

FIG. 9. *P-E* hysteresis loops of the 5 mol % Mn-doped $(1-x)BiFeO_3$–$xPbTiO_3$ (BF-100*x*PT) thin films on $Pt/TiO_x/SiO_2/Si$ substrates after heat treatment at 600 °C (measured at room temperature). (a) BF-20PT, (b) BF-30PT, (c) BF-40PT, and (d) BF-50PT.

than that applied for the $BF_{0.97}M_{0.03}$-30PT and $BF_{0.95}M_{0.05}$-30PT thin films could be applied, which suggests lower resistivity for breakdown of $BF_{0.99}M_{0.01}$-30PT films.

Fang *et al.*[33] reported the MnO_2 doping effect in decreasing the dielectric loss of iron-containing dielectrics, such as $Pb(Fe_{1/4}Sc_{1/4}Nb_{1/2})O_3$. Iron-containing ferroelectrics tend to exhibit a large dielectric loss, which is thought to correlate with a partial reduction of Fe^{3+} to Fe^{2+} ions during heat treatment. This decrease in dielectric loss is thought to be due to the compensation of the charge disproportion of Fe ions from Mn ion doping. The effect of Mn doping on the ferroelectric properties of the BF-30PT thin film was clearly observed, as shown in Fig. 8. For these thin films, a doped Mn ion can exist as Mn^{2+} and trap the hopping electrons between Fe^{3+} and Fe^{2+} in the BF-PT film. Higuchi *et al.*[34] reported the determination of valency and site occupation of Mn ions in the crystal structure for the Mn-doped $BiFeO_3$–$BaTiO_3$ (BF-BT) ceramics, observed by soft x-ray absorption spectroscopy. In this case, doped Mn ions are located at Fe sites and act as acceptors improving the electrical properties of the BF-BT ceramics. The same effect also seems to be observed in the current Mn-doped BF-PT thin films in this study.

Among the films in Fig. 8, the $BF_{0.95}M_{0.05}$-30PT thin film has relatively well-shaped hysteresis loops and the largest remanent polarization. Accordingly, the optimum Mn concentration is determined to be about 5 mol %. Figure 9 shows the *P-E* hysteresis loops of the 5 mol % Mn-doped BF-20PT, 30PT, 40PT, and 50PT thin films measured at room temperature. Mn doping of 5 mol % reduced the leakage component and improved the ferroelectric properties (higher P_r and lower E_c) of the BF-20PT, 40PT, and BF-50PT thin films, as well as those of BF-30PT thin films. Both 5 mol % Mn-doped BF-40PT and BF-50PT films exhibited hysteresis loops as good as those of 5 mol % Mn-doped BF-

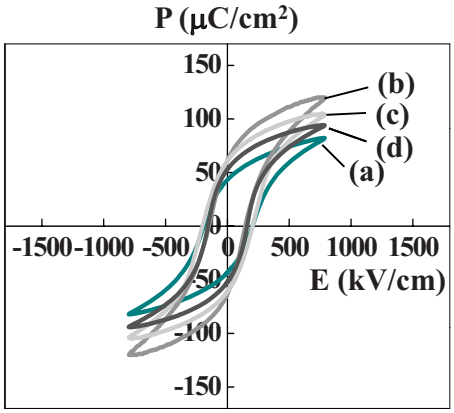

FIG. 10. (Color online) *P-E* hysteresis loops of the 5 mol % Mn-doped $(1-x)BiFeO_3-xPbTiO_3$ (BF-100*x*PT) thin films on $Pt/TiO_x/SiO_2/Si$ substrates after heat treatment at 600 °C (measured at −190 °C). (a) BF-20PT, (b) BF-30PT, (c) BF-40PT, and (d) BF-50PT.

30PT thin films near the MPB composition. The P_r and E_c of 5 mol % Mn-doped BF-20PT, 30PT, 40PT, and 50PT films were approximately 35, 40, 45, and 40 $\mu C/cm^2$, and 120, 100, 75, and 75 kV/cm, respectively. Measurement at low temperature was also performed, and the *P-E* hysteresis loops of the Mn-doped BF-PT thin films at −190 °C are shown in Fig. 10. Regardless of the film composition, all the thin films exhibited relatively saturated ferroelectric hysteresis loops with no leakage current component. Among these films, 5 mol % Mn-doped BF-30PT thin films showed the largest polarization similar to that of nondoped BF-PT thin films measured at −190 °C. The remnant polarization (P_r) of the 600 °C-prepared Mn-doped BF-30PT and BF-40PT thin films was almost the same value (65 $\mu C/cm^2$). The 600 °C-prepared BF-20PT and BF-50PT thin films exhibited smaller P_r values of approximately 45 and 55 $\mu C/cm^2$, respectively. When the applied electric field exceeded 1200 kV/cm, the 5 mol % Mn-doped BF-30PT thin films exhibited a P_r value of approximately 90 $\mu C/cm^2$. This value was obtained for polycrystalline thin films with no preferred orientation. Therefore, larger ferroelectricity is expected to be achieved by further control of the film orientation in the direction of polarization. Because BF-PT compounds are multiferroics, the magnetic properties of the BF-PT thin films are also important, and currently under investigation. We will report on the orientation control and multiferroic properties of the BF-PT thin films in the near future.

IV. CONCLUSIONS

Ferroelectric $(1-x)BiFeO_3-xPbTiO_3$ (BF-100*x*PT, $x=0.2$, 0.3, 0.4, 0.5) thin films with a thickness of 500 nm were synthesized by CSD. Perovskite $BiFeO_3-PbTiO_3$ single-phase thin films with a rms roughness value less than 4.0 nm could be fabricated by optimizing the processing conditions. Although the electrical resistivity was not sufficiently high around room temperature, the potential ferroelectricity of the synthesized films was revealed at low temperatures. Among the BF-PT thin films with various $PbTiO_3$ concentrations, the BF-30PT thin films were found to exhibit the largest P_r value (60 $\mu C/cm^2$) and E_c value (230 kV/cm) at −190 °C. The Mn-doped $BiFeO_3-PbTiO_3$ thin films, however, showed reduced leakage current density at higher electric fields and relatively well-shaped *P-E* hysteresis loops at room temperature. Mn doping of 5 mol % was the most effective in improving the ferroelectric properties of the $BiFeO_3-PbTiO_3$ thin films. The remanent polarization (P_r) and coercive field (E_c) of the 5 mol % Mn-doped $0.7BiFeO_3$-$0.3PbTiO_3$ films at room temperature were approximately 40 $\mu C/cm^2$ and 100 kV/cm, respectively. These results demonstrate that the $BiFeO_3-PbTiO_3$ thin films have excellent ferroelectric properties, comparable to or larger than those of lead zirconate titanate (PZT). This provides scope for the practical application of these materials in electronic thin-film devices using ferroelectricity.

ACKNOWLEDGMENTS

This work was supported by a Grant-in-Aid for Scientific Research (B), No. 19360297 from the Ministry of Education, Culture, Sports, Science and Technology, Japan.

[1] J. Wang, J. B. Neaton, H. Zheng, V. Nagarajan, S. B. Ogale, B. Liu, D. Viehland, V. Vaithyanathan, D. G. Schlom, U. V. Waghmare, N. A. Spaldin, K. M. Rabe, M. Wuttig, and R. Ramesh, Science **299**, 1719 (2003).
[2] G. A. Smolenskii and I. E. Chupis, Sov. Phys. Usp. **25**, 475 (1982).
[3] S. V. Kiselev, R. P. Ozerov, and G. S. Zhdanov, Sov. Phys. Dokl. **7**, 742 (1962).
[4] P. Fischer, M. Polomska, I. Sosnowska, and M. Szymanski, J. Phys. C **13**, 1931 (1980).
[5] F. Kubel and H. Schmid, Acta Crystallogr., Sect. B: Struct. Sci. **46**, 698 (1990).
[6] I. Sosnowska, T. Peterlin-Neumaier, and E. Steichele, J. Phys. C **15**, 4835 (1982).
[7] J. R. Teague, R. Gerson, and W. J. James, Solid State Commun. **8**, 1073 (1970).
[8] K. Y. Yun, D. Ricinschi, T. Kanashima, M. Noda, and M. Okuyama, Jpn. J. Appl. Phys., Part 2 **43**, L647 (2004).
[9] F. Bai, J. Wang, M. Wittig, J.-F. Li, N. Wang, A. P. Pyatakov, A. K. Zvezdin, L. E. Cross, and D. Viehland, Appl. Phys. Lett. **86**, 032511 (2005).
[10] H. Uchida, R. Ueno, H. Nakaki, H. Funakubo, and S. Koda, Jpn. J. Appl. Phys., Part 2 **44**, L561 (2005).
[11] S. K. Singh and H. Ishiwara, Jpn. J. Appl. Phys., Part 1 **45**, 3194 (2006).
[12] S. Yasui, H. Uchida, H. Nakaki, H. Funakubo, and S. Koda, Jpn. J. Appl. Phys., Part 1 **45**, 7321 (2006).
[13] F. Tyholdt, S. Jorgensen, H. Fjellvag, and A. E. Gunnaes, J. Mater. Res. **20**, 2127 (2005).
[14] Y. Noguchi, T. Matsumoto, and M. Miyayama, Jpn. J. Appl. Phys., Part 2 **44**, L570 (2005).
[15] Y. Noguchi, M. Soga, M. Takahashi, and M. Miyayama, Jpn. J. Appl. Phys., Part 1 **44**, 6998 (2005).
[16] Y. Wang and C.-W. Nan, Appl. Phys. Lett. **89**, 052903 (2006).
[17] V. R. Palkar, J. John, and R. Pinto, Appl. Phys. Lett. **80**, 1628 (2002).
[18] Y. P. Wang, L. Zhou, M. F. Zhang, X. Y. Chen, J. M. Liu, and Z. G. Liu, Appl. Phys. Lett. **84**, 1731 (2004).
[19] S. A. Fedulov, P. B. Ladyzhinskii, I. L. Pyatigorskaya, and Y. N. Venevtsev, Sov. Phys. Solid State **6**, 375 (1964).
[20] D. I. Woodward, I. M. Reaney, R. E. Eitel, and C. A. Randall, J. Appl. Phys. **94**, 3313 (2003).
[21] W. Sakamoto, H. Yamazaki, A. Iwata, T. Shimura, and T. Yogo, Jpn. J. Appl. Phys., Part 1 **45**, 7315 (2006).
[22] J.-R. Cheng and L. E. Cross, J. Appl. Phys. **94**, 5188 (2003).
[23] S. K. Singh, K. Sato, K. Maruyama, and H. Ishiwara, Jpn. J. Appl. Phys., Part 1 **45**, L1087 (2006).
[24] S. K. Singh, K. Maruyama, and H. Ishiwara, Appl. Phys. Lett. **88**, 262908 (2006).
[25] M. A. Khan, T. P. Comyn, and A. J. Bell, Appl. Phys. Lett. **91**, 032901 (2007).
[26] K. Morito, T. Suzuki, and M. Fujimoto, Jpn. J. Appl. Phys., Part 1 **40**,

5493 (2001).
[27]C.-F. Chung, J.-P. Lin, and J.-M. Wu, Appl. Phys. Lett. **88**, 242909 (2006).
[28]H. Naganuma and S. Okamura, J. Appl. Phys. **101**, 09M103 (2007).
[29]P. Zubko, D. J. Jung, and J. F. Scott, J. Appl. Phys. **100**, 114113 (2006).
[30]G. W. Pabst, L. W. Martin, Y.-H. Chu, and R. Ramesh, Appl. Phys. Lett. **90**, 072902 (2007).
[31]B. Nagaraj, S. Aggarwal, T. K. Song, T. Sawhney, and R. Ramesh, Phys. Rev. B **59**, 16022 (1999).
[32]F. Chen, Q. F. Zhang, J. H. Li, Y. J. Qi, C. J. Lu, X. B. Chen, X. M. Ren, and Y. Zhao, Appl. Phys. Lett. **89**, 092910 (2006).
[33]B. Fang, Y. Shan, K. Tezuka, and H. Imoto, Jpn. J. Appl. Phys., Part 1 **44**, 5030 (2005).
[34]T. Higuchi, W. Sakamoto, N. Itoh, T. Shimura, T. Hattori, and T. Yogo, Appl. Phys. Express **1**, 011502 (2008).